DOI 10.1007/s10946-018-9708-2
Journal of Russian Laser Research, Volume 39, Number 2, March, 2018

PACKAGING AND CHARACTERISTICS OF A TAPERED FIBER SENSOR FOR REFRACTIVE-INDEX MEASUREMENTS

Xingliu Hu,[1*] Zhaoxia Shi,[2] Yan Wang,[2] and Zhong Yang[1]

[1] *College of Intelligent Science and Control Engineering*
Jinling Institute of Technology
Nanjing 211169, Jiangshu, China

[2] *College of Information and Electric Engineering*
Anhui University of Technology
Ma'an Shan 243002, Anhui, China

*Corresponding author e-mail: xinghu8@163.com

Abstract

In this study, we demonstrate the design and fabrication of a tapered fiber sensor with a sensing application based on a new (high-sensitivity) package. We study the effect of various geometric parameters such as the uniform segment diameter, the uniform segment length, and the incident angle of the optical wave on the tapered fiber sensor sensitivity for evanescent sensing. Our study shows that high sensitivity of the tapered fiber can be realized by optimizing its parameters. In addition, we design a novel packaging of a tapered-fiber sensor, which can efficiently ensure a uniform stress and reduce the cross sensitivity caused by stress in liquid detection using a tapered fiber sensor. We report the experimental results obtained using this tapered fiber sensor for refractive-index measurements. As the refractive index of liquids varies from 1.417 to 1.423, the measurement results show that the refractive-index sensitivity of the tapered fiber sensor is as high as 4860 nm/RIU.

Keywords: microoptics, packaging, concentration, sensor.

1. Introduction

Following the development in all science fields, optical fiber technology, which has gradually matured, has been widely used in various fields owing to their extraordinary properties such as low insertion losses, high sensitivity, fast response, flexible structure, and others. The optical fiber application involves the detection of strain, pressure, temperature, and other physical parameters [1–3]. Some fiber characteristics such as small size and light weight provide easy packaging. However, they also easily break when used in harsh environment, in addition to being prone to cross sensitivity to strains and temperature.

Because of the characteristics of optical fibers, their packaging has become an essential factor for their practical applications. For concentration sensing, an ideal fiber package not only has to adapt to low concentration of analytes but also must be able to reduce the cross sensitivity to strains and temperature. For instance, much research effort has focused on the development of fiber packaging, which has many potential applications in optical communication and sensors, e.g., fiber Bragg grating [3–6], long-period grating pair [7–9], and tapered fiber [10–12] packaging. These techniques greatly optimize the optical performance stability.

Manuscript submitted by the authors in English on January 25, 2018.

In this work, we study the characteristics of tapered optical fibers, including the influence of geometric parameters and the structure of a tapered optical fiber on its sensitivity. A new tapered fiber sensor is also proposed. The experimental results demonstrate its high sensitivity in successfully detecting the refractive index of a levofloxacin lactate (LVF) solution.

2. Basic Principle

2.1. Structure of a Tapered Fiber

As a new type of optical fibers, tapered fibers are obtained by pulling cones of ordinary fibers. Tapering can expose the evanescent field to the environment, and it can be performed either by removing the cladding and then tapering the core or keeping both the core and cladding in place and tapering the entire fiber [13], which is adopted in the present study. Several methods for fabrication of tapered fibers with diameters of approximately a few micrometers have been implemented, such as flame drawing [14], indirect laser drawing [15], and chemical etching [16].

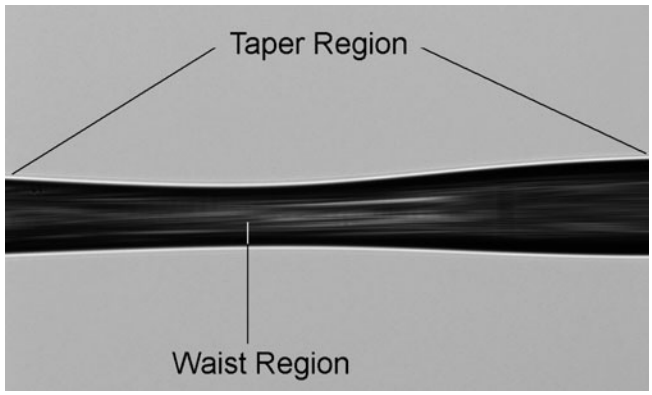

Fig. 1. Geometric structure of a tapered fiber.

In Fig. 1, we show a tapered fiber consisting of three regions: a convergent region with decreasing diameter, a waist region, and a tapered region with increasing diameter.

2.2. Principle of Detection by a Tapered Fiber

Because of the special structure of a tapered fiber, changes in the refractive index of the liquid lead to a change in the mode effective index when its waist region is immersed in liquid, which consequently results in a resonance shift and, thus, in spectrum changes. Mathematical expressions have been modeled for this condition.

In this study, we develop a new model, which considers the tapered fiber core and cladding as a new core, and the liquid as a new cladding. In this case, the model distribution can be regarded as a TP_{01} [17] model index. Thus, we can use a Gaussian approximation instead of the expression of the TP_{01} model index described as follows:

$$p_1/p_2 \approx 1 - \exp\left[-2(r_2/r_3)^2\right], \tag{1}$$

where p_1 and p_2 denote the optical power of the tapered fiber and the total power, and r_2 and r_3 denote the fiber-core and mode-field radii, respectively. Analyzing the step-index fiber, we can write the relationship between the mode-field and fiber-core radii as

$$r_3^2 = 2r_2^2/\ln(2\Delta k_0^2 n_f^2 r_2^2), \tag{2}$$

where Δ is the relative refractive-index difference expressed as $\Delta = (n_f - n_2)/n_f$, and n_f denotes the mode effective index of the tapered optical fiber. Here, n_2 denotes the refractive index of the liquid. Equations (1) and (2) yield

$$p_1/p_2 \approx 1 - 1/(c_1 - c_2 n_0), \tag{3}$$

where $c_1 = 2k_0^2 n_f^2 r_2^2$, $c_2 = 2k_0^2 n_f r_2^2$, and $k_0 = 2\pi/\lambda$, with λ denoting the wavelength of the light source.

The mode index of the tapered fiber is modeled using a symmetric planar waveguide model to ensure that not only the waist region of the tapered fiber is immersed in fluid but also the refractive index of the fluid is the same at both sides in the waist region. Using Eq. (3), we carry out the simulations to evaluate the linear relationship between the refractive index of the fluid and its transmission. We use a standard SMF-28 optical fiber in our experiments. The mode effective index n_f is 1.4654. We solve Eq. (3) in order to obtain the mode indexes for four values of r_2, namely, 3.5, 4.5, 5.5, and 6.5 μm, which represent the fiber core radii. In Fig. 2, we show the light transmission shift versus variations in the decrease in the external refractive index (from 1.30 to 1.43). The linear fitting of the experimental data indicates that the ratio of the optical power to the total power versus the increase in the fluid refractive index decreases, which indicates more light losses in the fluid. Therefore, the refractive index of the liquid can be calculated using the data on transmission. One can calculate the liquid concentration using the correspondence between the concentration and the refractive index.

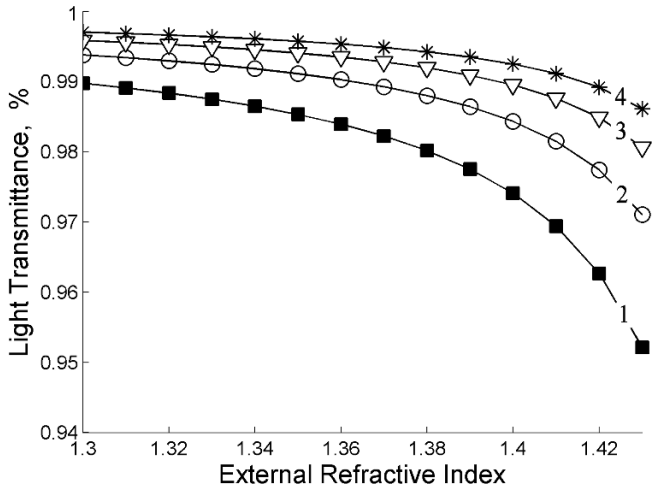

Fig. 2. Light transmissions through a tapered fiber versus the fluid refractive index at a fiber wavelength of 1,550 nm for four various values $r_2 = 3.5$ μm (curve 1), $r_2 = 4.5$ μm (curve 2), $r_2 = 5.5$ μm (curve 3), and $r_2 = 6.5$ μm (curve 4).

2.3. Sensitivity of a Tapered Fiber

According to the geometric structure characteristics of a tapered fiber, when the waist region, whose mode index is sensitive to the surrounding refractive index, is immersed in a liquid, it can be considered as a fiber-optic evanescent wave absorption sensor. Many geometric factors affect the sensitivity of the tapered fiber. When the refractive index of the fiber core is close to that of the cladding index, the fiber sensitivity reads

$$S = L\,\frac{d\gamma}{dc}\,, \tag{4}$$

where S is the fiber sensitivity, L is the effective length of the optical fiber, c is the molar absorption of the solution to be tested, and γ is the absorption coefficient of the fiber, which is

$$\gamma = \frac{\ln 10\varepsilon c\lambda n_0 \cos^2\theta}{2r_1\pi(n_1^2 - n_0^2)\sin\theta\sqrt{\sin^2\theta - (n_0/n_1)^2}}\,. \tag{5}$$

Here, ε is the liquid concentration, θ is the angle of incidence of the light on the core/cladding interface, n_1 and n_0 are the refractive indexes of the fiber core and cladding index, respectively, λ is the wavelength of the light source, and r_1 is the fiber-core radius.

We can rewrite Eq. (5) as follows:

$$\gamma = \alpha\varphi, \tag{6}$$

where α is the absorption coefficient of the test solution, and φ is a function related to the wavelength,

fluid refractive index, and the fiber geometry. The we can express α as

$$\alpha = 4\pi n_2^*/\lambda = \ln 10 \cdot \varepsilon c, \tag{7}$$

$$\varphi = \frac{\lambda n_0 \cos^2\theta}{2\pi r_1 (n_1^2 - n_0^2)\sin\theta\sqrt{\sin^2\theta - (n_0/n_1)^2}}\,. \tag{8}$$

In view of Eqs. (4) and (6), we arrive at

$$S = L\left[\alpha\frac{d\varphi}{dc} + \varphi\frac{d\alpha}{dc}\right]. \tag{9}$$

A condition exists where the refractive index of the liquid does not significantly change, namely,

$$S = L\varphi\left(\frac{d\alpha}{dc}\right) = \frac{\ln 10 L\lambda n_0\cos^2\theta}{2\pi\rho(n_1^2 - n_0^2)\sin\theta\sqrt{\sin^2\theta - (n_0/n_1)^2}}\varepsilon. \tag{10}$$

Equation (10) shows that the fiber sensitivity is influenced by many factors, which include not only the effective length of the optical fiber and the angle of incidence but also the operating wavelength and cladding index.

To clarify the effects of each factor on the tapered fiber, we carry out the simulations; in Fig. 3, we show the sensitivity of the tapered fiber versus the angle of incidence (which varies from 84° to 90°), with $L = 6$ m and $r_1 = 35$ μm. We can see that the sensitivity of the optical fiber decreases with increase in the angle of incidence, and the response tends to zero when the angle of incidence approaches a right angle.

Figure 3 a shows a comparison of the different curves, which indicates that an increase in the fiber wavelength (which varies from 545 to 1,345 nm) is expected to be accompanied by an increase in the sensitivity of the optical fiber. In Fig. 3 b, we show the variation in the fiber sensitivity with the angle of incidence and the refractive index of the solution, which varies from 1.30 to 1.386. The fitting result shows that an increase in the refractive index of the solution can be obtained with a higher sensitivity.

3. Device and Experiment

3.1. Package Structure of a Tapered Fiber

On the basis of the aforementioned theoretical research, we show that a higher sensitivity of a tapered fiber can be realized by optimizing the parameters of the tapered fiber. As a new type of fiber, a tapered fiber shows better performance than a common fiber, such as high fraction of evanescent fields, low optical loss through sharp bending, and so on. However, the tapered fiber suffers from some limitations because of its high-sensitivity characteristics in which the propagating-mode properties are changed with any change in the environment. To achieve better application, more packaging options are needed.

The packaging structure designed in this study is shown in Fig. 4. It has four fixed tables and is provided with a groove to house the tapered-fiber ends within the channel located at the base. In the encapsulation of the tapered optical fiber, the fiber must be placed in the groove with the two free ends fixed on the fixed tables to ensure that the stress is uniform. Thus, the cross sensitivity of the stress factor is reduced. The structure of the fixed table is shown in Fig. 5 a.

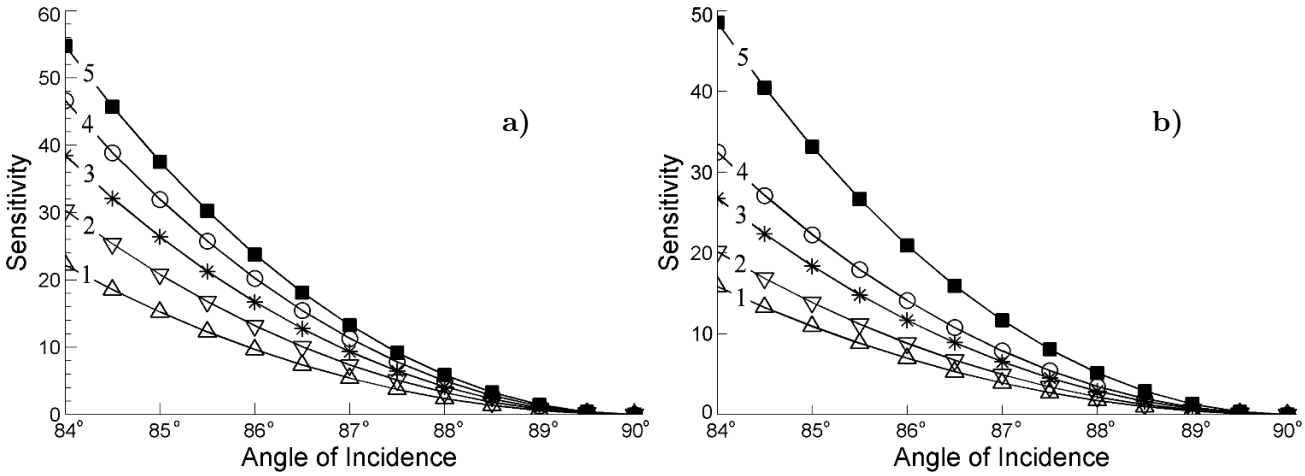

Fig. 3. Sensitivity of the tapered fiber versus the angle of incidence. Here, the sensitivity of the optical fiber with different wavelengths versus the angle of incidence at a refractive index of 1.36 (a) with $\lambda = 545$ nm (curve 1), $\lambda = 745$ nm (curve 2), $\lambda = 945$ nm (curve 3), $\lambda = 1,145$ nm (curve 4), and $\lambda = 1,345$ nm (curve 5), and the sensitivity of the optical fiber, which is immersed in different solutions with different refractive indices, versus the angle of incidence at a fiber wavelength of 1,550 nm (b) with $n_0 = 1.300$ mm (curve 1), $n_0 = 1.324$ nm (curve 2), $n_0 = 1.348$ nm (curve 3), $n_0 = 1.362$ nm (curve 4), and $n_0 = 1.386$ nm (curve 5).

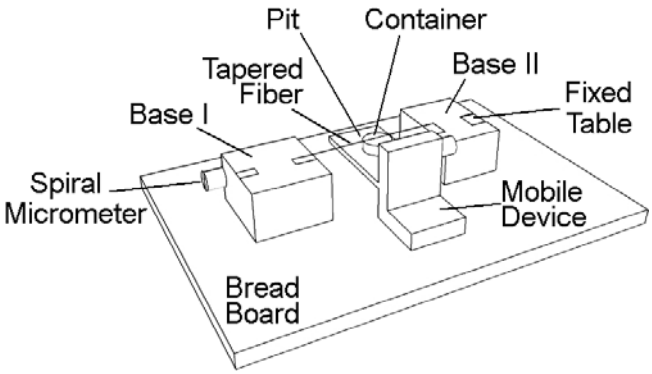

Fig. 4. Experimental setup in the laboratory.

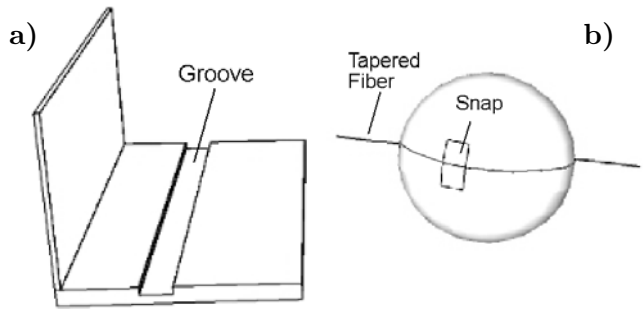

Fig. 5. Component structure. Here, a schematic diagram of the fixed table (a) and a schematic diagram of the transparent container (b).

A mobile device is placed between the two bases whose materials are generally chosen as engineering plastics such as polyamide. The material must have good characteristics such as high mechanical strength, high heat resistance, low coefficient of friction, and so on. A pit is provided through the mobile device to embed the bottom part of the transparent container. The pit size needs to match the size of the transparent container.

The structure of the transparent container used to contain the liquid sample is shown in Fig. 5 b. The top and bottom of the transparent container are provided with a movable piston to control the injection and discharge of the liquid. It serves to regularly clean the tapered fiber during the detection process. The piston is reusable and very strong. In addition, the upper part of the transparent container is inscribed with a horizontal line to always ensure the same amount of liquid. To keep the optical fiber under the same hydraulic pressure always, its lower part is symmetrically provided with two grooves whose width is approximately 150 μm, which are used to embed the tapered fiber. The upper and lower parts of the transparent container are stitched to a snap to ensure that liquid does not flow out during the measurement process.

According to the measurement requirements, the bases and the movable device are each equipped with many spiral micrometers that can precisely adjust the spacing between the bases and movable device. Adjustment of the spiral micrometer can change the stress on the tapered fiber, and different adjustments will vary the stress on the tapered optical fiber. Therefore, when the positions of the bases and the movable device are determined and the tapered optical fiber is fixed, the rotating spiral micrometer is no longer needed in the entire detection process.

3.2. Refractive Index Detection by a Tapered Fiber

We measured the LVF solution at room temperature using a tapered fiber sensor. During the measurements, the temperature was maintained at 25°C to avoid shifts in the wavelength due to temperature variations. All readings were taken several minutes after the tapered-fiber sensor was immersed in the solution. The refractive index of the LVF solution was varied from 1.417 to 1.423. The waist region of the tapered optical fiber sensor was soaked in the solution to be measured.

In Fig. 6, we see that when the solution refractive index was varied, the position of the dip wavelength of the tapered fiber sensor was altered. As the refractive index n_2 of the environmental solution increases, the transmission spectrum of the tapered fiber structure moved toward the direction of increasing wavelength.

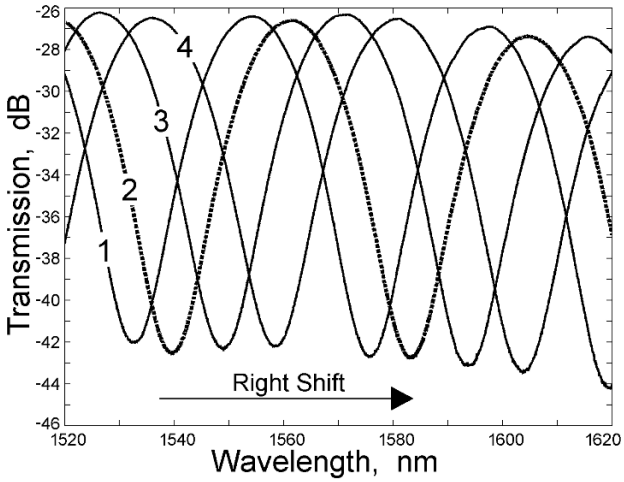

Fig. 6. Spectral response of the tapered fiber sensor under different refractive indices $n = 1.417$ (curve 1), $n = 1.417$ (curve 2), $n = 1.419$ (curve 3), $n = 1.421$ (curve 4), and $n = 1.423$ (curve 5).

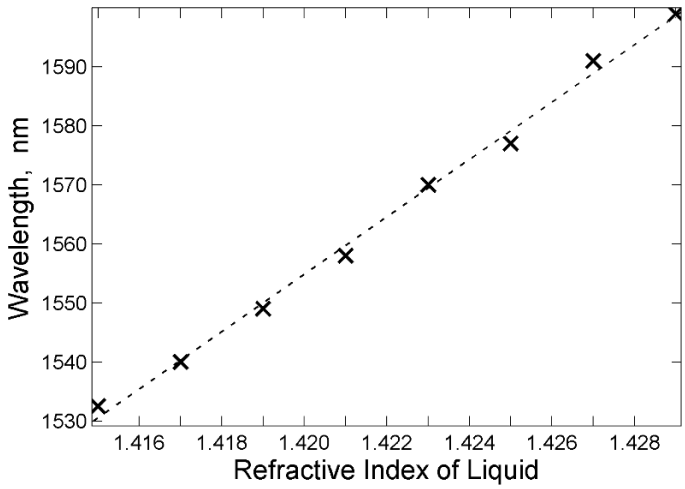

Fig. 7. Relationship between the refractive index and the dip wavelength, in view of Eq. (11), through the coordinate positions, with the direct line as a fitting curve.

The experimental data points were fitted using polynomial regression. The relationship between the variation in the dip wavelength and the solution refractive index was obtained using the linear fitting equation shown in Fig. 7. The linear fitting equation reads

$$f(x) = 4,860\,x - 5,356. \tag{11}$$

Here, x is the solution refractive index, and $f(x)$ is the dip wavelength of the tapered fiber sensor. As the solution refractive index varied from 1.417 to 1.431, the dip wavelength of the sensor increased linearly from 1,532 to 1,599 nm with a sensitivity of 4,860 nm/RIU.

4. Conclusions

In this study, we investigated the effect of various geometric parameters of a tapered fiber sensor on its sensitivity. We designed a new packaging of tapered optical fiber, which provides the advantages of ease in fabrication and insensitivity to fluctuations in temperature and strain. We investigated a tapered fiber sensor based on this structure for refractive index measurements by monitoring the dip wavelength of the spectra. The refractive index sensitivity of the sensor was 4,860 nm/RIU with an excellent linearity, which shows that the sensor performed well. In the future, this device can potentially be applied to the concentration detection.

Acknowledgments

This work was supported by the National Natural Science Foundation under Grants Nos. 61201109, 51309001 and 51275239, as well as by the General Program of Jiangsu Province's Natural Science Foundation BK20171114, Qing Lan Project, Jinling Institute of Technology's Talent Introduction Project No. Jit-rcyj-201604, Jinling Institute of Technology's Research Training Project No. Jit-fhxm-201606, National Science Foundation of the Higher Education Institutions of Jiangsu Province under Grants Nos. 16KJB510010 and 17KJB120003, the China Scholarship Council, Anhui Province's Natural Science Key Project No. KJ2017A041, Anhui Province's Natural Science under Grant No. 1308085ME79, and Anhui Province's Science and Technology Project No. 12010402c182.

References

1. H. F. Lima, P. F. Antunes, J. de Lemos Pinto, and R. N. Nogueira, *IEEE Sensors J.*, **10**, 269 (2010).
2. V. V. Spirin, M. G. Shlyagin, S. V. Miridonov, et al., *Opt. Lasers Eng.*, **32**, 497 (1999).
3. K. Imade, D. Koyama, and I. Akiyama, *J. Acoust. Soc. Am.*, **137**, 2424 (2015).
4. Y. L. Lo and C. P. Kuo, *J. Lightwave Technol.*, **21**, 1377 (2003).
5. G. Woyessa, K. Nielsen, A. Stefani, et al., *Opt. Express*, **24**, 1206 (2016).
6. F. Marignetti, E. D. Santis, S. Avino, et al., *IEEE Trans. Industr. Electron.*, **63**, 2796 (2016).
7. F. Y. M. Chan and K. Yasumoto, *International Conference on Electromagnetics Advance Applications*, IEEE, Torino (2007).
8. S. W. James and R. P. Tatam, *Meas. Sci. Technol.*, **14**, 49 (2003).
9. T. Allsop, L. Zhang, and I. Bennion, *Opt. Commun.*, **191**, 181 (2001).
10. Yoon, Min Seok, S. Park, and Y. G. Han, *J. Lightwave Technol.*, **30**, 1156 (2012).
11. A. Layeghi, H. Latifi, and O. Frazao, *IEEE Photon. Technol. Lett.*, **26**, 1904 (2014).
12. S. C. Kang, M. K. Song, J. T. Moon, and H. T. Lee, *Lasers and Electro-Optics Society Meeting*, IEEE, Maryland (1997).
13. A. Leung and P. M. Shankar, *Sens. Actuators B: Chem.*, **125**, 688 (2007).
14. T. A. Birks and Y. W. Li, *J. Lightwave Technol.*, **10**, 432 (1992).
15. T. E. Dimmick, G. Kakarantzas, T. A. Birks, and P. S. Russell, *Appl. Opt.*, **38**, 6845 (1999).
16. A. Dudus, R. Blue, and D. Uttamchandani, *IEEE Sensors J.*, **13**, 1594 (2013).
17. D. J. Richardson, E. Koukharenko, F. Xu, et al., *Adv. Opt. Photon.*, **1**, 107 (2009).